Electrochemical-Impedance-Spectroscopy Study of Corrosion of Fe and Ni with Molten ZnCl2-KCl Coating in Air at 673K

T. J. Pan^{1,2*}, Y. F. Lin¹, J.Hu¹ and C.L Zeng²

¹Department of Materials Science and Engineering, Jiangsu Polytechnic University, Changzhou, 213164, P.R. China; ²State Key Laboratory for Corrosion and Protection, Institute of Metal Research, The Chinese Academy of Science, Shenyang 110016, P.R. China;

(Received August 29, 2009: final form September 18, 2009)

ABSTRACT

The corrosion of Fe and Ni covered with a molten film of 0.55ZnCl₂-0.45KCl was examined in air at 673K by the electrochemical-impedance spectroscopy (EIS) technique. Meanwhile, the impedance behavior for Fe and Ni immersed in the deep salt was also studied for comparison. The EIS for Fe beneath a thin salt film and in deep salt both showed a semicircle at high frequency and a line at low frequency, indicating a diffusioncontrolled reaction, but with much larger impedance in deep salt. The corrosion of Ni beneath a salt film was composed of two stages with different EIS features. The initial Nyquist plots also showed the characteristics of a diffusion-controlled reaction, as for the impedance features of Ni in deep salt, but converted into two capacitance loops at longer times. Equivalent circuits representing the corrosion of Fe and Ni were proposed to fit the corresponding impedance spectra and electrochemical parameters in the equivalent circuit were calculated.

Keywords: Fe, Ni, ZnCl₂-KCl, EIS, impedance models

Tel: 086-0519-86330099, Email: tjpan2005@gmail.com

1. INTRODUCTION

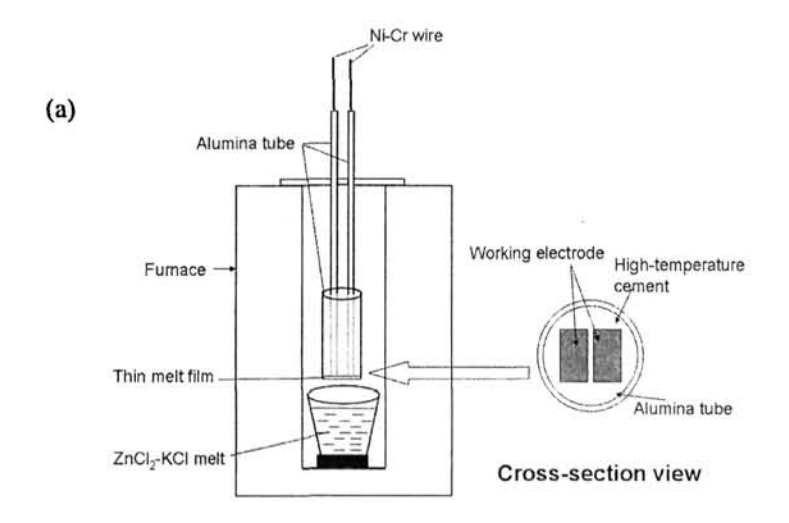
The corrosion problems in waste incineration plants are usually very severe because heavy metal (Sn, Pd, Zn) and alkali metal (Na, K) chlorides and sulfates frequently occur as molten state on the surface of metallic materials in the operation temperature range of superheater tubes /1/. The fused salt-induced hot corrosion has been identified as the main degradation in waste incineration plants. This type of corrosion is actually an accelerated oxidation in a high temperature gaseous environment of a material whose surface is coated by a thin fused salt film and differs largely from the corrosion of the materials in deep salt. This high temperature attack by molten salts is mainly electrochemical in nature, and thus may be investigated by electrochemical techniques.

In recent years, Electrochemical-impedance spectroscopy (EIS) is increasingly becoming a powerful tool for elucidating electrochemical reaction processes because this technique may provide useful information for clarifying complicated electrode processes /2-4/. Additionally, an extra advantage of the EIS techniques is that use of only very weak signals during measurement does not disturb the corrosion system to be investigated.

^{*}Correspondent: T.J. Pan

In general, a successful application of the EIS technique requires suitable models for fitting the impedance spectra. Zeng et al. /5/ ever used EIS technique to investigate the molten-salt corrosion behavior by proposing four models to describe the scaling features of metallic materials. In addition, some papers concerning application of EIS technique in the study of hot corrosion have also been published /6-10/, hereinto a two-electrode system seemed more suitable for studying hot corrosion behavior beneath a thin salt

film by using EIS /9,10/. However, the studies on hot corrosion by using EIS technique are still scanty. In this study, the corrosion of Fe and Ni beneath a fused ZnCl₂-KCl film at 673K was studied by using EIS technique. For comparison, their impedance behaviors in deep salt were also tested. This paper mainly focuses on the impedance measurement and the establishment of impedance models for corrosion of Fe and Ni beneath molten chlorides film.



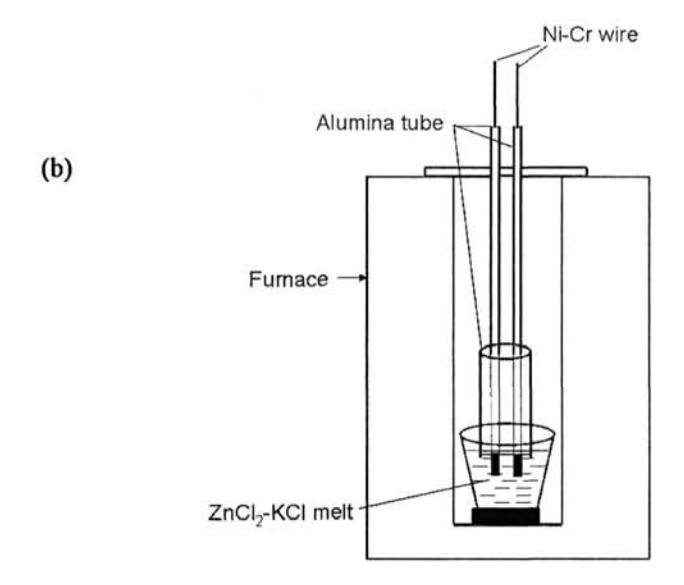


Fig. 1: Schematic diagram of test apparatus for corrosion beneath thin salt film and cross-section view of two electrode arrangement (a) and for corrosion in deep molten salt (b)

2. EXPERIMENTAL PROCEDURES

The materials employed in this study were pure iron and nickel. A two-electrode (two working electrodes, WE) system was used for the impedance measurement. Cross-section view of two electrode arrangement and the experimental assembly are shown in Figure 1.

The working electrodes were prepared as follows. Samples of the two materials were machined into a size of 10 x 10 x 5 mm³, and then each sample was ground down to 600[#] SiC paper. A Ni-Cr wire was spot welded to one end of the specimens for electric connection. Two specimens very closely spaced were sealed in an alumina tube by high temperature cement, with one side of 10 x 5 mm² uncovered. The exposed surfaces of the specimens were in the same plane. Top view of two-electrode arrangement is shown in Figure 1. After the cement was dried at room temperature, it was further solidified at 473K for 24h. The working electrode surface was polished again on 600[#] SiC paper, degreased and dried.

A mixture of 0.55ZnCl₂-0.45KCl (molar ratio) was applied in the present study. A total of 150g of the salt mixture were dried in an alumina crucible at 473K for 24 h in air. Then, the furnace was heated to 673K. In

order to produce a thin fused salt film on the electrode surface, the electrode arrangement was immersed briefly into the melt, then withdrawn and kept above the melt, as shown in Figure 1. This process was repeated after 12h to ensure the presence of a thin salt film on the electrode. The actual amount of the thin salt film was about $2 \text{ mg/cm}^2 = 20 \text{ g/m}^2$ in this work.

Electrochemical impedance measurements up to 24 h were performed at open-circuit potential in air between 0.01 and 1 x 10⁵ Hz with a M398 impedance system, composed of a Princeton Applied Research (PAR) 5210 lock-in amplifier and a PAR 263 potentiostat interfaced through an IEEE 488 bus to a compatible computer. A fast Fourier transform (FFT) technique was employed for frequencies from 0.01 to 1.13 Hz to increase measurement speed and lower the degree of perturbation to the cell. The amplitude of input sine signal was 10mV. A commercial software (ZSimpWin) developed by Princeton Applied Research was used to fit the impedance spectra. In the end, the corroded samples were examined by Scanning Electron Microscopy (SEM) coupled with an Energy-Dispersive X-ray microanalysis system (EDX).

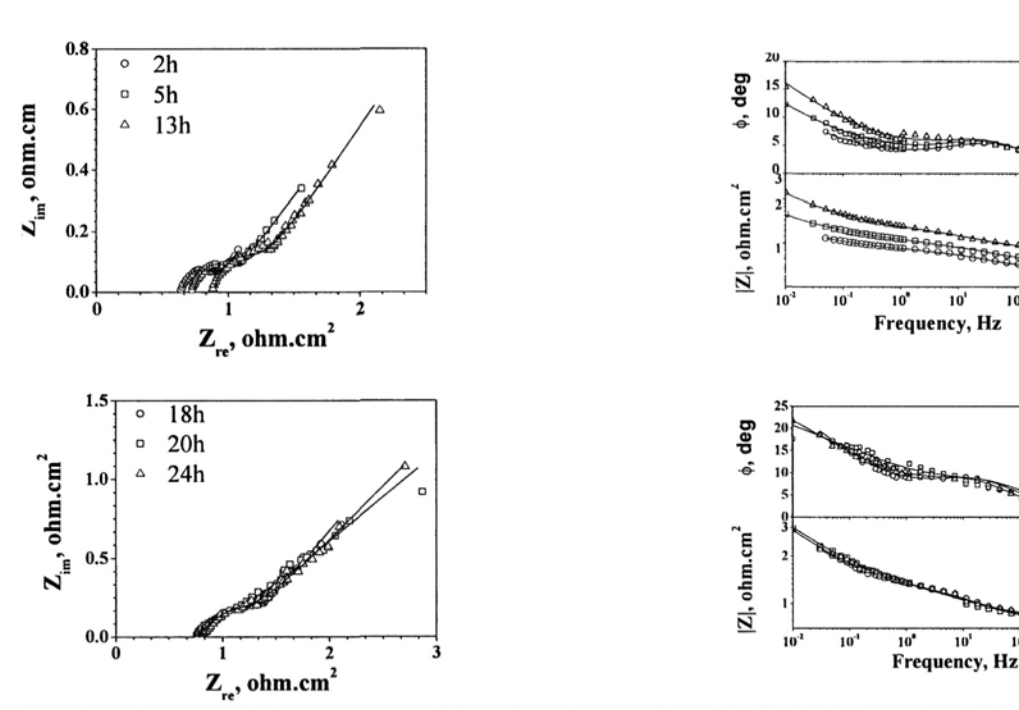


Fig. 2: Nyquist and Bode plots for corrosion of iron beneath a molten ZnCl₂-KCl film at 673K in air after different exposure times. Symbol: experimental data; line: simulation data.

2h

□ 5h

13h

18h

20h

24h

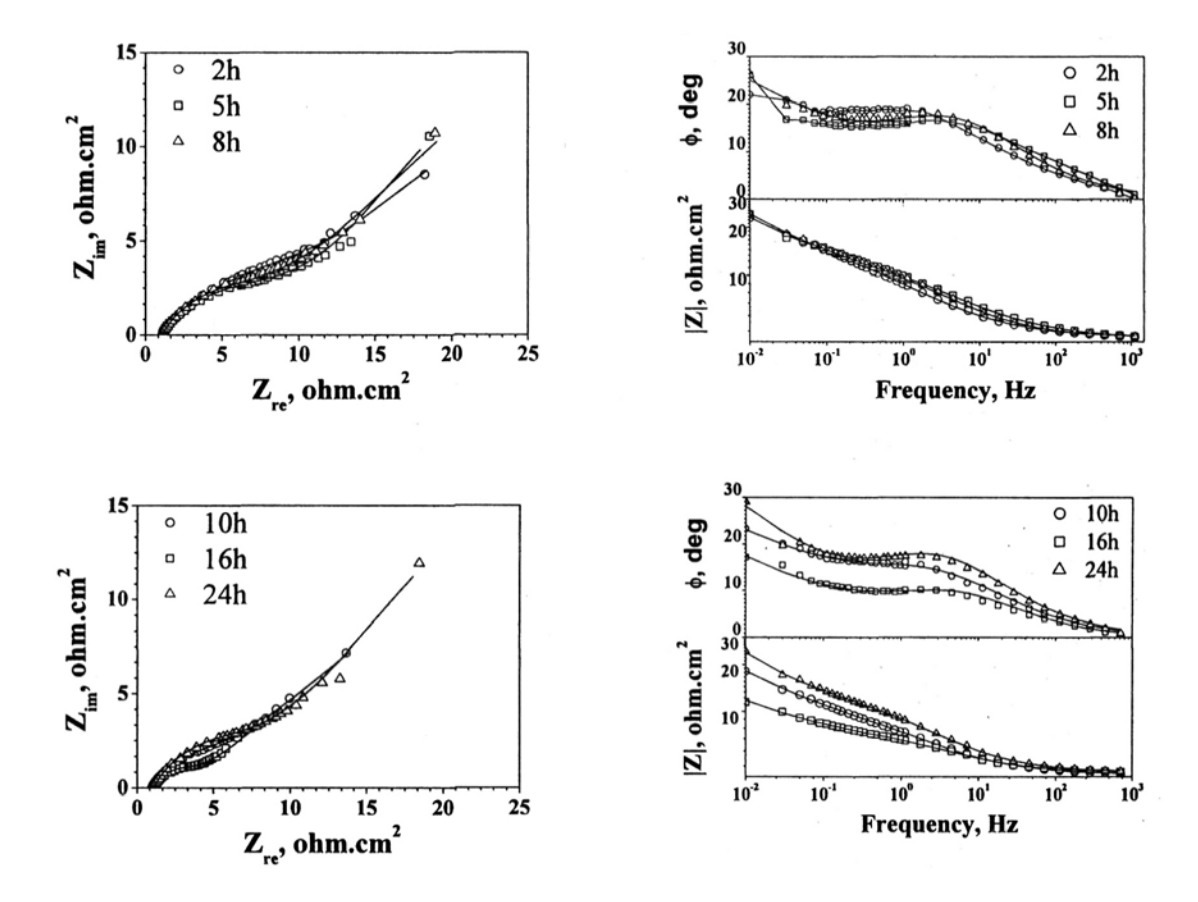


Fig. 3: Nyquist and Bode plots for corrosion of iron in deep molten ZnCl₂-KCl mixture at 673K in air after different exposure times. Symbol: experimental data; line: simulation data.

3. RESULTS AND DISCUSSIONS

3.1 EIS measurements

The typical Nyqusit and Bode plots for corrosion of Fe beneath a thin fused salt film and in deep salt after different exposure time are shown in Figs. 2 and 3, respectively. The features of the impedance spectra for iron under two different conditions are very similar during the whole experimental duration. The Nyquist plots are composed of a depressed semi-circle at high frequency section and a line at low frequency section, representing a diffusion-controlled reaction. The corresponding Bode plots show only a time constant. But the impedances | Z | for iron in deep salt (Figure 3) are larger than that beneath salt film (Figure 2) by more than an order of magnitude.

The corrosion of nickel beneath a salt film is composed of two stages with different impedance features, as shown in Figure 4. The initial Nyquist plots before 3h have the characteristics of diffusioncontrolled reaction, as for the whole corrosion of nickel in the deep salt (Figure 5), i.e., a small capacitive loop at high-frequency section and a line at low frequency part. After exposure of 3h, the Nyquist plots changed into two capacitance loops, i.e., a much larger semicircle at low frequency and a small depressed semicircle at high frequency. Furthermore, the corresponding Bode plots show two time constants. Although the high-frequency time constant is not very obvious, the low-frequency time constant can be distinguished well from the corresponding Bode plots. In the end, the impedance of Ni in deep salt is much larger than beneath salt film.

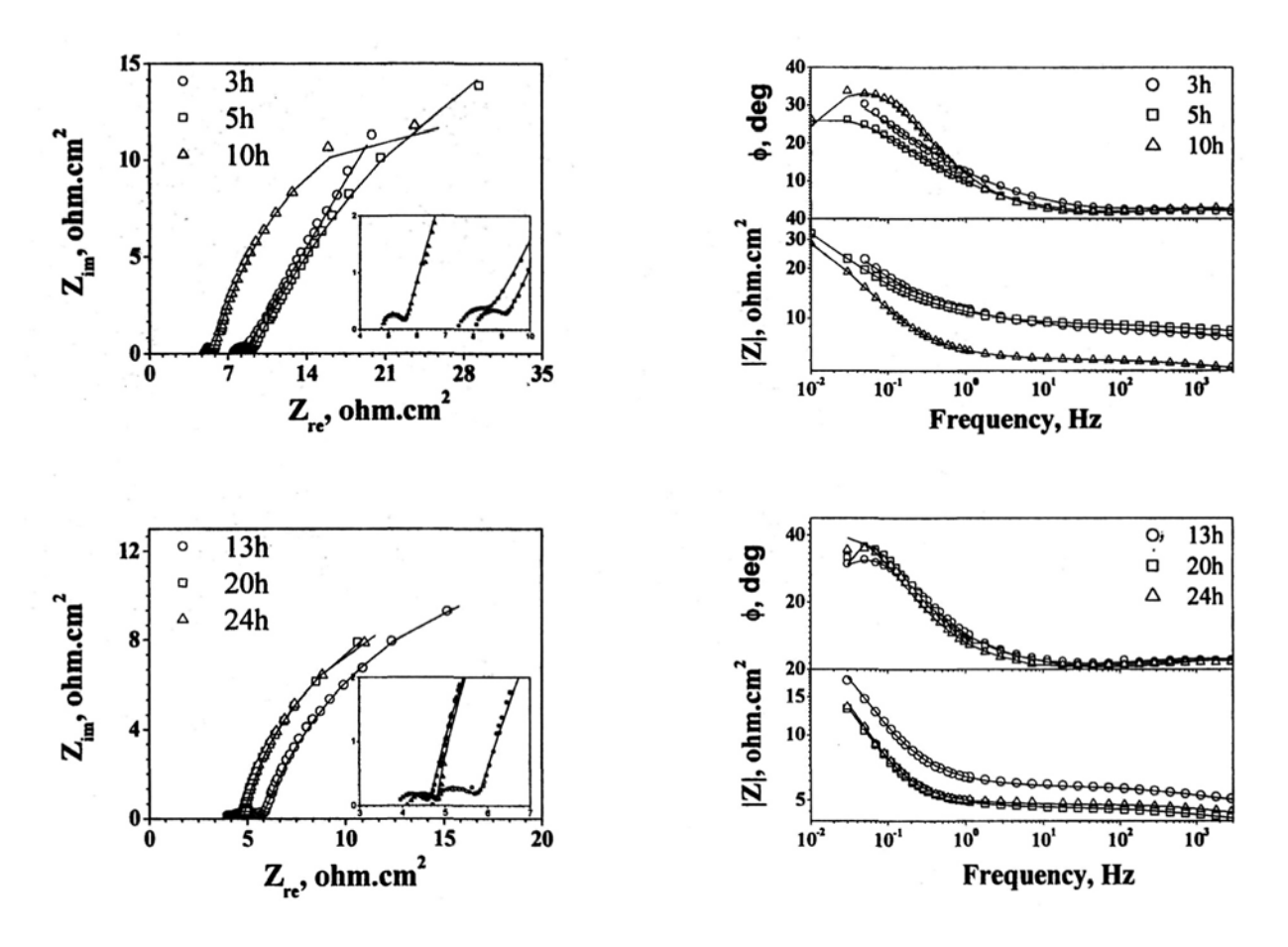


Fig. 4: Nyquist and Bode plots for corrosion of nickel beneath a molten ZnCl₂-KCl film at 673K in air after different exposure times. Symbol: experimental data; line: simulation data.

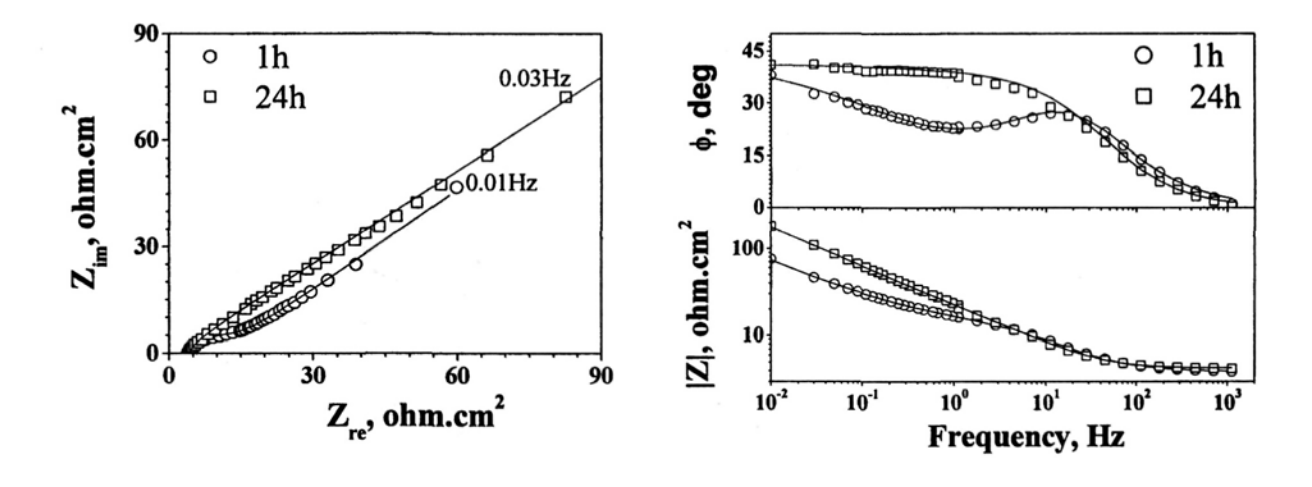
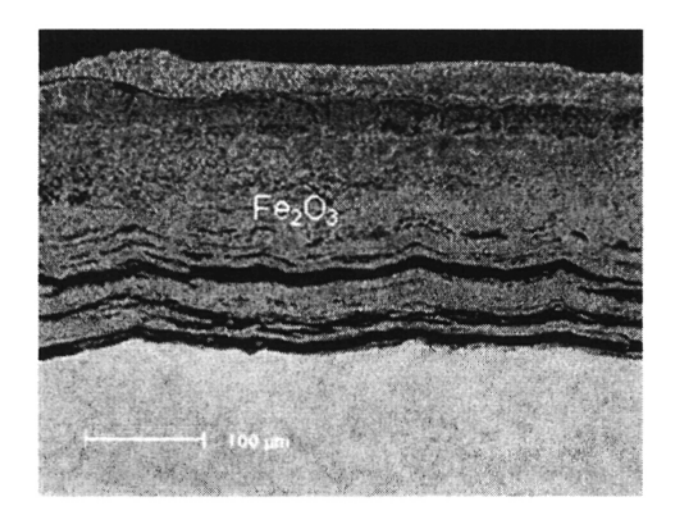


Fig. 5: Nyquist and Bode plots for corrosion of nickel in deep molten ZnCl₂-KCl mixture at 673K in air after different exposure times. Symbol: experimental data; line: simulation data.

3.2 Scale morphology

Figure 6 showed the typical morphology for cross sections of iron corroded below a fused salt film and in deep salt. The scale formed beneath a salt film was mostly Fe₂O₃, which was rather thick, porous and exhibited distinctive separations in the scale. A finegrained Fe oxide containing a small amount of Zn (4-5at.%) and Cl (2-3 at.%) in the outer region of this scale was detected by EDX. The scale formed in the deep salt was also iron oxide (Fe₂O₃), mostly possibly from the

oxidation of FeCl₂ in air, The scale was substantially similar to that formed beneath a salt film, but much thinner. Only a small amount of FeCl₂ can be detected at scale/iron interface because a large amount of FeCl₂ from the dissolution of iron in chlorides substantially changed into the corresponding iron oxide (Fe₂O₃) in air when the corroded samples was drew out from deep salt, which is mainly because the oxide is the stability phase in air according to the phase diagrams /11/.



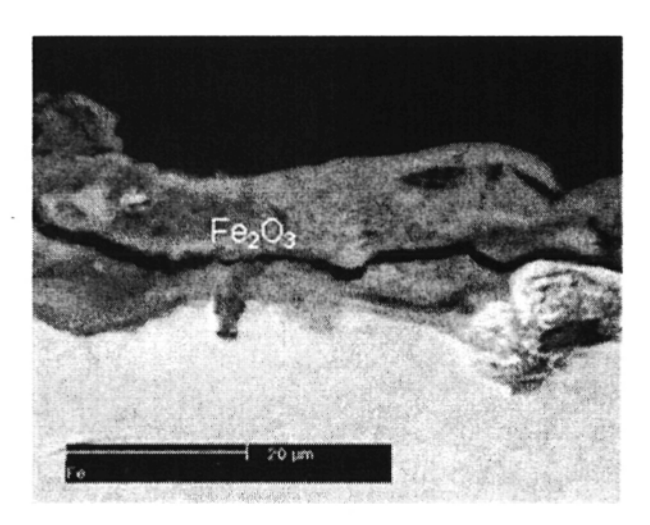


Fig. 6: Micrographs for cross sections of iron at 673K in air for 24h beneath salt film (a) and in deep salt (b).

The corrosion of nickel beneath a salt film produced the porous NiO scale containing some K, Zn and Cl, as shown Figure 7. In addition, a small amount of chlorine (3-4 at.%) was detected at the scale/substrate interface. However, in deep salt nickel only dissolved very slowly as form of Ni²⁺. Thus no cross section of nickel in the deep melt was showed here.

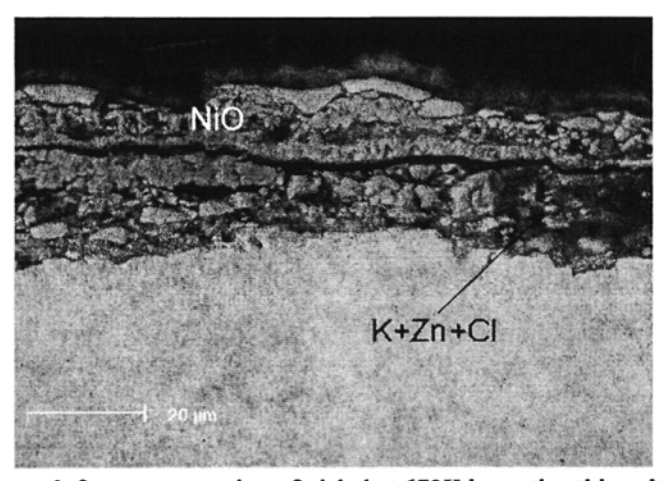


Fig. 7: Micrograph for a cross section of nickel at 673K beneath a thin salt film for 24h.

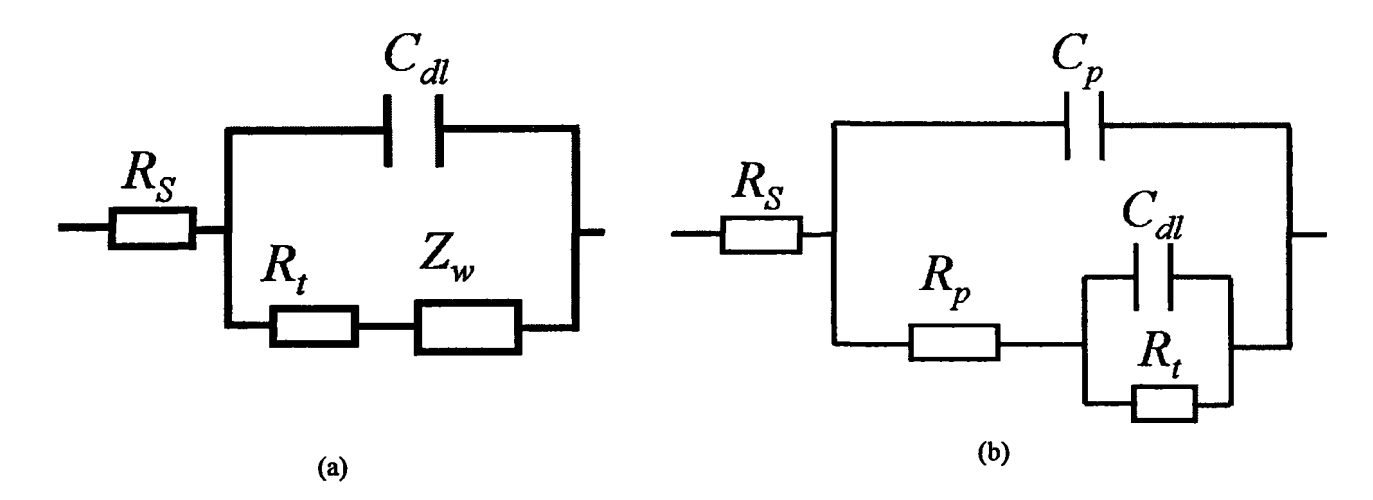


Fig. 8: Equivalent circuit representing the corrosion of iron and nickel in ZnCl₂-KCl mixture at 673K in air.

3.3 Impedance model for iron

The Nyquist plots for the corrosion of iron beneath fused $ZnCl_2$ -KCl film and in deep molten salt obviously show the features of diffusion-controlled reaction. Thus, an equivalent circuit of Figure 8a was proposed to fit the impedance plots. In Figure 8a, R_s represents the electrolyte resistance, R_t and C_{dl} represent the charge-transfer resistance and the double-layer capacitance, respectively, Z_w are the diffusion-induced Warburg resistance. In the fitting procedure, C_{dl} was replaced with constant phase angle element (CPE) Q because of the dispersion effect. Thus, the total electrochemical impedance for the circuit of Fig.8a can be expressed by Eq.(1)

$$Z = R_s + \frac{1}{Y_{ut} (j\omega)^{n_{dt}} + \frac{1}{(R_t + Z_w)}}$$
 (1)

where Y_{dl} and n_{dl} are constants representing the element Q_{dl} . The Warburg resistance Z_w can be expressed by Eq. (2)

$$Z_{w} = A_{w} (jw)^{n_{w}} \tag{2}$$

Where A_w is the modulus of Warburg resistance, and n_w is the Warburg coefficient, $0 > n_w \ge -0.5$, relating to the diffusion direction of oxidants. When n_w is equal to -0.5, the diffusion direction of oxidants is parallel to the concentration gradient of oxidants, and in Nyqusit plot

the slop of line at low frequency is equal to 1. When- $0.5 < n_w$, the diffusion direction of oxidants deviates from the concentration gradient of oxidants, i. e., the existence of "tangential diffusion". Accordingly, the slop of the line at low frequency in Nyquist plot is less than 1. In molten-salt corrosion, the "tangential diffusion" may be related to the porosity of the scale. The electrochemical parameters in Eq. (1) were obtained by fitting the experimental data based on equivalent circuit of Figure 8a, and listed in Tables 1 and 2. From the Nyquist plots in Figures 2 and 3, it can be seen that the fitting is good.

Table 1 show that the parameters R_t and Y_{dl} slightly fluctuate with the exposure time, except that the value of A_w slightly increased with time. The changes may be related to the slight fluctuation of the corrosion system. In Table 2, Y_{dl} and A_w also slightly change with immersion time, but R_t tends to decrease with time. Furthermore, A_w and R_t of Table 2 are larger than those of table 1 by more than a order of magnitude, indicating the diffusion of oxidants in deep salt is more difficulty than beneath salt film. Moreover, the charge transfer resistance R_i in Tables 1 and 2 is of the same magnitude as the modulus of the Warburg A_w , further indicating that the diffusion-induced impedance cannot be neglected in the corrosion processes. In the end, n_{dl} in two tables both greatly deviate 1, showing the presence of a dispersion effect, which is a notable feature for molten salt corrosion.

Table 1
Fitting results of impedance spectra of Fe beneath salt film in air at 673K

time (hour)	R_s $(\Omega.cm^2)$	R_t (Ω .cm ²)	Y_{dl} (Ω^{-1} .cm ⁻² S ⁻ⁿ)	n _{dl}	$A_{w,dl}$ $(\Omega.cm^2 S^n)$	-n _w
2	0.64	0.26	0.196	0.58	0.150	0.38
5	0.73	0.32	0.178	0.60	0.214	0.39
10	0.83	0.37	0.183	0.55	0.341	0.38
13	0.87	0.39	0.166	0.56	0.385	0.38
18	0.78	0.44	0.115	0.63	0.610	0.39
20	0.76	0.51	0.139	0.60	0.714	0.40
24	0.81	0.44	0.152	0.61	0.667	0.39

Table 2
Fitting results of impedance spectra of Fe in deep melt in air at 673K

time (hour)	R_s $(\Omega.cm^2)$	R_t (Ω .cm ²)	Y_{dl} $(\Omega^{-1}.cm^{-2} S^{-n})$	n_{dl}	$A_{w,dl}$ $(\Omega.cm^2 S^n)$	-n _w
2	1.02	11.42	4.80e-2	0.55	4.21	0.43
5	0.94	10.61	3.30e-2	0.55	3.38	0.50
8	1.07	7.56	2.55e-2	0.63	4.79	0.44
10	0.93	5.22	4.61e-2	0.61	4.44	0.40
16	1.09	6.68	3.95e-2	0.67	2.02	0.39
24	1.13	6.04	5.81e-2	0.66	3.52	0.45
30	1.07	8.12	3.21e-2	0.63	4.03	0.50

Iron exhibited some different features of cross section morphology under fused salt film and deep salt, which is attributed to the different supply of oxygen between beneath fused salt film and deep molten salt. In general, oxygen can easily reach the surface of iron to contribute the rapid conversion of formed FeCl₂ into Fe₂O₃ beneath a salt film according to the following reactions:

$$2FeCl_2 + \frac{3}{2}O_2 = Fe_2O_3 + 2Cl_2 \tag{3}$$

Thus, the corrosion of iron under salt film is considerably rapid; the corrosion procedure is controlled by the diffusion of gaseous FeCl₂ and oxygen through the porous scales /12-14/. However, in deep salt iron is only oxidized according to the following anodic reaction:

$$Fe = Fe^{2+} + 2e^{-} \tag{4}$$

At the same time, the corresponding cathodic reaction only occur as follows:

$$\frac{1}{2}O_2 + 2e - = O^{2-} \tag{5}$$

However, the solubility of oxygen is considerably small in chlorides, the supply of oxygen control the cathodic reaction. Thus, the whole corrosion of iron in deep salt is limited by the supply of oxygen at the cathodic reaction. So iron in deep salt dissolved slowly only as the type of Fe²⁺ in deep salt, not like the rapid corrosion of Fe beneath salt coating.

where Y_{dl} and n_{db} and Y_p and n_p are also constants representing the parameters Q_{dl} and Q_p , respectively.

The Nyquist plots in Figures 4 and 5 show clearly that the fitting are fairly good, indicating that the proposed equivalent circuit is reasonable. The

3.4 Impedance model for nickel

The impedance spectra for the initial corrosion of nickel beneath fused ZnCl₂-KCl film, similar to those of nickel in deep salt during the whole duration of the corrosion tests, also show the features of diffusion-controlled reaction, so they can be again represented by the equivalent circuit shown in Figure 8a.

However, with extended times the Niquist plots for corrosion of nickel beneath salt film changed into two capacitances, i.e., a much larger semicircle at low frequency and a small depressed semicircle at high frequency. The change of the impedance spectra may be associated with the growth of porous scales on the surface of nickel. At this stage the molten salt can penetrate inward along the micropores in the scale to the metal matrix to induce electrochemical reaction. This typical corrosion can be represented by the equivalent circuit of Figure 8b, where R, represents again the electrolyte resistance, C_{dl} and R_{t} represent the doublelayer capacitance and the charge-transfer resistance at the electrolyte/metal interface formed by the inward penetration of molten salts along pores, respectively. C_p and R_p represent the porous scale capacitance and the pore resistance, respectively. Considering the dispersion effect, C_{dl} and the C_p are replaced by constant angle element (CPE) Q in the fitting procedure. The total electrochemical impedance Z can be expressed by Eq. (6):

$$Z = R_{s} + \frac{1}{Y_{p} (j\omega)^{n_{p}} + \frac{1}{R_{p} + \frac{1}{Y_{dl} (jw)^{n_{dl}} + \frac{1}{R_{l}}}}}$$
(6)

electrochemical parameters in Eqs (1), (2) and (6) can be obtained by fitting the impedance spectra based on the equivalent circuit of Figure 8, and are listed in Tables 3 and 4, respectively.

 Table 3

 Fitting results of the impedance spectra of Ni beneath salt film in air at 673K

time (h)	R_s (Ω .cm ²)	R_t (Ω .cm ²)	Y_{dl} $(\Omega^{-1}.cm^{-2} S^{-n})$	n _{dl}	$A_{w,dl}$ (Ω .cm ² S ⁿ)	- <i>1</i> 11 ₁₁	R_p (Ω .cm ²)	$(\Omega^{-1}.\text{cm}^{-2}\text{S}^{-n})$	n_{p_1}
3	7.45	1.05	1.85e-3	0.72	8.71	0.50			
5	8.09	1.19	0.0023	0.70		\ <u></u>	59.52	0.1406	0.58
8	8.48	1.49	0.0016	0.70			54.05	0.173	0.63
10	4.73	0.87	0.0027	0.67			37.53	0.172	0.72
13	4.72	0.91	0.0014	0.73			49.56	0.191	0.68
20	3.99	0.64	0.0016	0.79			29.82	0.311	0.80
24	4.18	0.58	0.0010	0.81			35.80	0.310	0.79

Table 4
Fitting results of impedance spectra of Ni in deep melt in air at 673K

time (h)	R_{γ} (Ω .cm ²)	R_t (Ω .cm ²)	Y_{dl} $(\Omega^{-1}.cm^{-2} S^{-n})$	n _{dl}	$A_{u,dl}$ (Ω .cm ² S ⁿ)	-H _u
1	3.88	9.64	4.083e-3	0.81	16.99	0.48
2	3.93	11.52	2.851e-3	0.83	21.83	0.48
4	4.03	12.74	2.092e-3	0.86	38.80	0.46
6	4.03	12.25	1.961e-3	0.83	46.75	0.46
9	4.03	2.62	2.251e-3	0.90	28.37	0.36
12	4.24	3.14	1.527e-3	0.87	43.01	0.43
16	4.18	2.82	2.034e-3	0.87	53.79	0.45
22	4.43	4.67	1.991e-3	0.97	45.27	0.49
24	4.26	2.67	2.172e-4	0.93	49.95	0.46

From Table 3, it can be seen that the medium resistance R_r underwent slight changes with exposure time, possibly related to changes of the salt film on the samples. A_{rr} is much larger than R_r , indicating the diffusion limited the initial corrosion process. But the scale resistance R_p gradually tends to decrease with

time, indicating the protection of the porous scale become worse and worse; the small value of R_t indicated the electrochemical reaction is very fast. n_{tll} and n_p also significantly deviate from 1, demonstrating the existence of obvious dispersion effects.

From Table 4, it can be seen that A_w is much larger than R_h indicating the diffusion is the rate-limiting step for the corrosion of nickel in deep salt; Furthermore, n_w deviates from -0.5, indicating the presence of "tangential diffusion" during corrosion. R_l tends to decrease with time, which also means that the electrochemical reaction become faster.

In this study, nickel is oxidized in fused ZnCl₂-KCl mixture according to the following anodic reaction:

$$Ni = Ni^{2+} + 2e^{-} \tag{7}$$

At the same time, the corresponding cathodic reaction will occur as follows:

$$\frac{1}{2}O_2 + 2e - = O^{2-} \tag{8}$$

The Ni²⁺ formed during corrosion procedure may diffuse outward through the molten salt film. At the gas/melt interface, O²⁻ and Ni²⁺ will precipitate as a porous oxide by the following reaction /15/:

$$Ni^{2+} + O^{2-} = NiO (7)$$

The activity of oxygen decrease in molten salt because oxygen take part in the reduce reaction at the cathodic region. However, in whole corrosion process the anodic reaction of nickel precedes very easy, so it is impossible that the anodic reaction of nickel become rate-controlled reaction. Thus, this initial corrosion of nickel is controlled by the diffusion of oxidants through the molten salt film, in agreement with the presence of features typical of diffusion-controlled reactions in the corresponding electrochemical impedance spectra. After formation of porous NiO scale, the oxidants need to diffuse along the micropores in the scale to react with the metal, rather than diffusing through the salt film as during the first stage. The corrosion process during the second stage is controlled by the diffusion through the micropores in the scale. Therefore, the impedance spectra for the corrosion of nickel after the initial stage present a depressed semicircle at high-frequency and a large semicircle at low frequency. This change of impedance is closely related to the growth of porous scales.

The distinguished difference of impedance spectra exists between under salt film and in deep salt, which is related to the different supply of oxidants to the cathodic reaction under two conditions. In the high temperature molten salt system, the rapid anodic reaction needs to consume a large amount of oxidants. However, the solubility of oxygen in chlorides is very small; the insufficient supply of oxygen to the cathodic reaction retards the whole electrochemical reaction, so the diffusion of oxidants becomes rate-limiting step. But the transport of oxygen through salt film becomes relative easier than in deep salt. So nickel corroded faster under salt film than in deep salt, which is approved by the fact that the impedance of Ni in deep salt is larger than that beneath salt film. In addition, the solubility measurements of oxide scales in molten NaCl-KCl mixtures by Ishitsuka et al. /16/ showed that NiO is less soluble than the Fe and Cr oxides. Thus, it is easier to reach saturation in molten chlorides for NiO than for Fe and Cr oxides. Therefore, nickel-based alloys are better candidate materials than iron-based materials for a good resistance against chlorides deposits.

4. CONCLUSIONS

The electrochemical impedance spectra for the corrosion of iron beneath molten ZnCl₂-KCl film and in deep salt both showed a diffusion-controlled corrosion process, i.e., a small semicircle at high frequency and a line at low frequency. The corrosion of nickel beneath fused ZnCl₂-KCl film is composed of two stages with different impedance spectra. The initial Nyquist plots have the characteristics of a diffusion-controlled reaction, as for corrosion of nickel in deep salt, but are composed of two capacitance loops at second stage; the change of impedance spectra may be associated with the growth of porous scale at longer times. In the end, the impedance for iron and nickel in deep salt are larger than that beneath salt film, which may be related to the considerable low solubility of oxygen in the chlorides.

ACKNOWLEDGEMENTS

The authors acknowledge financial support by the high education natural scientific foundation of Jiangsu province, P.R. China under Contract 08KJB430003, and the natural scientific foundation of Jiangsu province, P.R. China under Contract SBK200930394, and by the science and technology project foundation of Changzhou city, P.R. China under Contract CE2008089.

REFERENCES

- H. J. Grabke, E. Reese, M. Spiegel, Corros. Sci., 37, 1023-1043 (1995).
- 2. A. Nishikata, Y. Ichihara, T. Tsuru, *Corros. Sci.*, 37, 897-911 (1995).
- 3. A. Nishikata, Y. Ichihara, T. Tsuru, *Electrochim. Acta.*, 41, 1057-1062 (1996).
- A. Nishikata, Y. Yamashita, H. Katayama, T. Tsuru,
 A. Usami, K. Tanabe, H. Mabuchi, *Corros. Sci.*, 37, 2059-2069 (1995).

- Electrochemical-Impedance-Spectroscopy Study of Corrosion of Fe and Ni with Molten ZnCl₂-KCl Coating in Air at 673K
- 5. C. L. Zeng, W. Wang, W. T. Wu, Corros. Sci., 43, 787-801 (2001).
- G. Gao, F.H. Stott, J.L. Dawson, D.M. Farrel, Oxid. Met., 33, 79-94 (1990).
- 7. X.J. Zheng, R.A. Rapp, *J. Electrochem. Soc.*, **140**, 2857 (1993).
- 8. Y. M. Wu, R. A. Rapp, *J. Electrochem. Soc.*, **138**, 2683-2690 (1991).
- 9.C.L. Zeng, T. Zhang, *Electrochim. Acta.*, **49**, 1429-1433 (2004).
- C.L. Zeng, J. Li, *Electrochim. Acta.*, **50**, 5533-5538 (2005).
- Y.S. Li, Y. Niu and W. T. Wu, *Mater. Sci. Eng.*, A345, 64-71 (2003).
- 12.Y, Ihara, H. Ohgame, K. Sakiyama, and K. Hashimoto, *Corros. Sci.*, **21**, 805-817 (1981).
- 13. R. J. Fruhan, *Metallurgical Transactions*, 3, 2585-2596 (1972).
- 14. Z. A. Foroulis, ANTI-Corrosion, 1, 4-12 (1988).
- 15.A Zahs, M Speigel, H J Grabke, Corros. Sci., 42, 1093-1122 (2000).
- Ishitsuka and K. Nose, Mater. Corrosion, 51, 177-181 (2000).